



RESEARCH ARTICLE

10.1002/2016JA023586

An analysis of magnetic reconnection events and their associated auroral enhancements

Key Points:

- A strong correlation exists between the location of magnetic reconnection in the magnetotail and auroral enhancements
- Short-lived localized auroral enhancements are as likely to occur during the substorm process as in isolation of a substorm
- No significant dependence of enhancement location on local or upstream conditions is found

Correspondence to:

N. A. Case,
n.case@lancaster.ac.uk

Citation:

Case, N. A., A. Grocott, S. E. Milan, T. Nagai, and J. P. Reistad (2017), An analysis of magnetic reconnection events and their associated auroral enhancements, *J. Geophys. Res. Space Physics*, 122, doi:10.1002/2016JA023586.

Received 18 OCT 2016

Accepted 14 FEB 2017

Accepted article online 18 FEB 2017

©2017. The Authors.

This is an open access article under the terms of the Creative Commons Attribution License, which permits use, distribution and reproduction in any medium, provided the original work is properly cited.

N. A. Case¹ , A. Grocott¹, S. E. Milan² , T. Nagai³ , and J. P. Reistad⁴

¹Department of Physics, Lancaster University, Lancaster, UK, ²Department of Physics and Astronomy, University of Leicester, Leicester, UK, ³Department of Earth and Planetary Sciences, Tokyo Institute of Technology, Tokyo, Japan, ⁴Department of Physics and Technology, University of Bergen, Bergen, Norway

Abstract An analysis of simultaneous reconnection events in the near-Earth magnetotail and enhancements in the aurora is undertaken. Exploiting magnetospheric data from the Geotail, Cluster, and Double Star missions, along with auroral images from the IMAGE and Polar missions, the relationship between a reconnection signature and its auroral counterpart is explored. In this study of 59 suitable reconnection events, we find that 43 demonstrate a clear coincidence of reconnection and auroral enhancement. The magnetic local time (MLT) locations of these 43 reconnection events are generally located within ± 1 h MLT of the associated auroral enhancement. A positive correlation coefficient of 0.8 between the two MLT locations is found. The enhancements are localized and short-lived ($\tau \leq 10$ min) and are as likely to occur during the substorm process as in isolation of a substorm. No significant dependence of the reconnection or auroral enhancement location on the dusk-dawn components of the solar wind velocity (V_y), IMF (B_y) or local B_y or V_y , as measured by the reconnection-detecting spacecraft, is found.

1. Introduction

Magnetic reconnection in the terrestrial magnetosphere has been a topic of interest for several decades and is the fundamental driving process in the classical Dungey cycle picture of energy transport in the magnetosphere [Dungey, 1961]. In the quasi-steady state Dungey cycle, reconnection in the Earth's magnetotail takes place in a region $\sim 100 R_E$ downtail of the Earth. However, when sufficient reconnection takes place between the interplanetary magnetic field (IMF) and the dayside magnetosphere, the open magnetic flux content of the tail increases and reconnection can then occur much closer to the Earth [Nagai et al., 2005]. Studies have shown that although this near-Earth reconnection can be observed at various distances out in the magnetotail [e.g., Nishida and Nagayama, 1973], most takes place in a region located $\sim 20\text{--}30 R_E$ downtail [e.g., Nagai et al., 1998]. Solar wind conditions, particularly the solar wind velocity and strength of the southward component of the IMF (B_z), influence the radial distance of the reconnection location [Nagai et al., 2005].

It is well established that magnetic reconnection in the Earth's magnetotail occurs in association with expanded enhancements in the aurora known as auroral substorms [e.g., Hones, 1979; Nishida et al., 1981; Baker et al., 1996], although the exact relationship is still under investigation [McPherron, 2016]. Furthermore, studies such as Grocott et al. [2004] have demonstrated that reconnection is linked with enhancements in the aurora that do not quite develop into substorms, commonly known as pseudo-breakups [Akasofu, 1964]. We also know that reconnection plays an important role in other distinct forms of auroral enhancements. For example, poleward boundary intensifications (PBIs) are driven by fast flows in the magnetotail, resulting from reconnection and move equatorward through the oval over time [Lyons et al., 1999].

Previous studies have demonstrated that the upstream IMF conditions affect the auroral substorm onset location. The different components of the IMF have been shown to influence the onset location, and substorm expansion, in different ways. For example, the latitude of substorm onset is related to the history of the IMF B_z component [e.g., Milan et al., 2010] whereas the azimuthal (local time) location of substorm onset has been shown to be dependent upon the IMF B_y component [e.g., Liou et al., 2001].

Although previous studies have directly linked reconnection and associated fast flows in the magnetotail to enhancements in the aurora [e.g., Nakamura et al., 2001; Borg et al., 2007; Angelopoulos et al., 2008;

Zhang *et al.*, 2010], the nontrivial nature of finding reconnection events has meant that most were individual case studies. Ieda *et al.* [2001], however, compared 24 plasmoids with ultraviolet observations of auroral brightenings. The term “plasmoid” describes a bipolar B_z in the plasma sheet that is accompanied by hot plasma moving tailward at a speed of at least 200 km s^{-1} [Ieda *et al.*, 1998] and is thought to be the result of magnetic reconnection [Ieda *et al.*, 2001]. B_y inferring that plasmoids are indeed the result of reconnection, Ieda *et al.* [2001] demonstrated that reconnection drove localized enhancements in the aurora but that such enhancements were not always guaranteed. Further investigation by Ieda *et al.* [2008] then demonstrated that auroral breakup was always accompanied by a coincident near-Earth reconnection event.

The difficulty in performing such comparative studies is that they require both magnetospheric spacecraft to detect reconnection and auroral imagers to detect enhancements in the aurora. While there are several suitable magnetospheric missions currently in operation (e.g., Geotail, Cluster, THEMIS, and MMS), whole auroral oval imaging satellites have been sparse and, in fact, none are currently operational today. As such the comparative studies have always been on small data samples.

In this study we perform a comprehensive investigation of the relationship between reconnection events in the magnetotail, detected using an automated signature detection routine and auroral enhancements observed in whole auroral oval images. We consider the relationship for different auroral enhancement characteristics, enhancements occurring during different substorm phases, and different in situ and solar wind plasma and magnetic field conditions. We find that reconnection is almost always associated with a discernible auroral enhancement and that these enhancements are often localized and short-lived. Reconnection occurs equally before and after substorm onset but also frequently occurs without an associated large-scale substorm auroral breakup. The dusk-dawn components of the upstream solar wind velocity (V_y) and IMF (B_y), and of the local magnetospheric V_y and B_y , appear to have no influence on the location of the reconnection site or the auroral enhancement.

2. Data

Detections of magnetic reconnection and corresponding enhancements in the aurora require both in situ measurements of the reconnection region and large-scale imaging of the aurora. In this study, auroral images are taken from the Polar and Imager for Magnetopause-to-Aurora Global Exploration (IMAGE) missions with in situ measurements of the reconnection region collected using the Geotail, Cluster, and Double Star missions. Associated solar wind and IMF data are provided by NASA's OMNIWeb service and lagged to the Earth's bow shock.

The Polar satellite was launched in February 1996 as one of two spacecraft from the Global Geospace Science program [Acuña *et al.*, 1995]. The satellite was placed in a highly elliptical orbit (86° orbital inclination) with an orbital period of approximately 17 h and remained operational until 2008. The orbital configuration of the spacecraft varied over time and resulted in the majority of auroral images being captured during the years 1996–1999 (Northern Hemisphere) and 2007 (Southern Hemisphere) [Liou, 2010]. The Visible Imaging System (VIS) [Frank *et al.*, 1995] Earth camera used in this study, was designed to capture images of the nightside aurora in the 124–149 nm range, with the optically thick oxygen line at 130.4 nm responsible for the majority of the camera response [Frank and Sigwarth, 2003]. The resolution of the camera was about 70 km from an altitude of $8 R_E$. The 256×256 pixel images have an exposure time of approximately 12 s and a cadence of 54 s.

The IMAGE spacecraft [Burch, 2000] was launched in March 2000 and remained operational until December 2005. Placed in a polar orbit (90° orbital inclination) with apogee at $7 R_E$ and perigee at $0.2 R_E$, the spacecraft was able to capture images of the whole auroral oval, predominantly in the northern polar region, when its altitude was greater than $4 R_E$. The Far Ultraviolet Wideband Imaging Camera (WIC) [Mende *et al.*, 2000] captured auroral images of 256×256 pixels in size with a spatial resolution of approximately 100 km at apogee. The camera was sensitive to the spectral region of 140–190 nm which best represents auroral emissions (mainly from the Lyman-Birge-Hopfield nitrogen emission) while also minimizing dayglow contamination [Mende *et al.*, 2000]. Images were captured every 2 min.

The Geotail spacecraft was launched in July 1992 and remains operational to this date. Onboard instruments include the Magnetic Field (MGF) [Kokubun *et al.*, 1994] and Low Energy Particle (LEP) [Mukai *et al.*, 1994] experiments. The MGF experiment incorporates two fluxgate magnetometers, located on a deployable mast, which provide measurements of the local magnetic field at a resolution of 16 vectors/s (later reduced to

4 vectors/s). The LEP experiment is composed of three different sensors, which include the Energy per charge Analyzer (LEP-EA). LEP-EA measures the three-dimensional velocity distributions of electrons and ions in the energy-per-charge range of a few eV/q to 43 keV/q [Mukai *et al.*, 1994]. Velocity moments are obtained over four spins (12 s).

The Cluster mission is a constellation of four identical spacecraft. Included in the suite of instruments on board each spacecraft is the magnetic field experiment, composed of two fluxgate magnetometers (FGM) [Balogh *et al.*, 1997] and the Cluster Ion Spectroscopy (CIS) experiment [Rème *et al.*, 2001]. The FGM instruments are still operational on all spacecraft and provide 5 vectors/s measurements of the local magnetic field. The CIS instrument provides 4 s resolution measurements of the velocity and temperature of different ion species; however, the instrument is now only operational on two of the four spacecraft.

The Double Star mission, launched in December 2003, followed on from the Cluster mission and was composed of two identical spacecraft with much of the same instrumentation as Cluster [Liu *et al.*, 2005]. However, the Double Star spacecraft did not include a full CIS instrument suite and instead only used a hot ion analyzer to measure ion distributions. Of the two Double Star spacecraft, only spacecraft one ventured into the reconnection region and so it is only this spacecraft that is used in this study.

In this study, all magnetospheric spacecraft data are presented using the Geocentric Solar Magnetospheric (GSM) coordinate system and are resampled to identical time tags with a 12 s cadence.

3. Method

The magnetospheric spacecraft data are first filtered to the region of the magnetotail where near-Earth tail reconnection is known to occur: $-50R_E \leq X \leq -10R_E$, $|Y| \leq 15R_E$, and $|Z| < 5R_E$ (in GSM coordinates) [e.g., Nagai *et al.*, 1998]. The Nagai *et al.* [1998] reconnection signature detection criteria, detailed below, are applied to the data to determine the occurrence of any reconnection signatures, known as Fast Tailward Flow Events (FTFEs). Once a reconnection signature is detected, subsequent detections by any of the other magnetospheric spacecraft within a 30 min window are ignored. We note that the lifetime of fast flows is of the order of 10–20 min [Angelopoulos *et al.*, 1992; Ieda *et al.*, 1998; Cao *et al.*, 2006] and fast flow group sizes in the near-Earth region are small [Frühhauff and Glassmeier, 2016], so this 30 min window ensures that the detected FTFEs are distinct from each other.

3.1. Reconnection Signatures

Direct detection of magnetic reconnection is not a trivial task. The reconnection region, located roughly 20–30 R_E downstream in the magnetotail [Nagai *et al.*, 1998], is estimated to have a width of only one ion inertial length in the tailward direction [Nagai *et al.*, 2011; Zenitani *et al.*, 2012] and spans approximately 6 R_E in the dawn-dusk direction [Nagai *et al.*, 2015]. As a result, the chances of a spacecraft (or even multiple spacecraft) passing through this region can be quite slim. However, by identifying several key reconnection signatures, it becomes increasingly likely that evidence of magnetic reconnection having occurred can instead be found. Nagai *et al.* [1998] determined that the following criteria produced accurate reconnection signatures:

1. $B_z < 0$ nT.
2. $V_x \leq -300$ km/s.
3. $\beta \geq 1$.

Criteria 1 and 2 identify FTFEs, with an associated reversal in the local magnetic field, which are indicative of magnetic reconnection having occurred somewhere earthward of the spacecraft. We note that the ion velocity measurements recorded by Geotail are made using the assumption that all ions are protons [Mukai *et al.*, 1994]. As such, the Cluster proton velocity data, rather than ion data, are also used. Since Double Star can only record the velocity of hot ions, we are forced to use the hot ion velocity rather than the proton velocity data from that spacecraft.

A plasma beta (i.e., the ratio of the plasma pressure to the magnetic pressure) $\beta > 1$ (criterion 3) indicates that the spacecraft is located within the plasma sheet. This criterion ensures that we only detect signatures of reconnection that have taken place in the plasma sheet, rather than other fast flow events occurring elsewhere in the magnetotail that are not the result of reconnection.

We determine the location, in magnetic local time (MLT), of the reconnection signature using the location of the detecting spacecraft in the magnetotail (e.g., $\tan^{-1}(Y_{\text{GSM}}/X_{\text{GSM}})/15$) rather than, for example, mapping

the spacecraft to the ionosphere and determining the MLT of its footprint. We note that by comparing the magnetospheric location to the MLT of an auroral enhancement, we are assuming that the near-Earth magnetotail magnetic field roughly takes the form of a dipolar field. Studies have shown that this can sometimes not be the case [e.g., *Reistad et al.*, 2016], and so we tested using the *Tsyganenko and Sitnov* [2005] magnetic field model (TS05) to map the spacecraft location to the ionosphere. In the majority of cases the mapping did not provide significantly different MLT values from just using the spacecraft location, and in some cases the model did not produce a mapped footprint or instead produced MLTs which were significantly different than what would be expected from the spacecraft position. We thus chose to use the unmapped spacecraft location for determining the reconnection MLT.

3.2. Associated Auroral Enhancements

A period spanning 2 h preceding and 30 min following each FTFE detection is determined. This range is chosen based on average substorm timescales [e.g., *Frey et al.*, 2004]. If auroral imaging data are available for this period, they are manually inspected to determine if any auroral enhancements are present within ± 5 min of the FTFE. We note that *Ieda et al.* [2001] found that their auroral brightenings occurred within ± 3.5 min of their plasmoid reconnection events and thus a maximum difference of ± 5 min seems reasonable.

In the following, we categorize the auroral enhancements based on their features (i.e., spatial and temporal extent) and timing with respect to the substorm process. We utilize the substorm onset criteria of *Frey et al.* [2004] to determine whether an enhancement is just a localized event or the start of a substorm, and at what point of the substorm process the enhancement occurs. Specifically, a substorm onset is defined as clear local brightening of the aurora that expands to the poleward boundary of the auroral oval. Additionally, the brightening must span at least 20 min in local time and not occur within 30 min of a previous substorm onset [*Frey et al.*, 2004]. Activity that shows some expansion but does not reach the poleward boundary of the auroral oval is often termed a pseudo-breakup [*Frey et al.*, 2004].

In our results, all enhancements not meeting the [*Frey et al.*, 2004] substorm criteria have a lifetime of < 10 min and a maximum expansion/spatial extent of 5° in latitude and 30 min in MLT. To avoid any ambiguity with existing definitions of pseudo-breakups, we define these events as “short-lived localized enhancements.” In four cases multiple enhancements are evident at the same time; we term these “several distinct localized enhancements,” with the auroral enhancement having the closest MLT match to the reconnection MLT chosen for comparison. Additionally, there are some events where no coincident auroral enhancement and FTFE are observed, and some in which significant auroral activity is already present, e.g., a substorm expansion already in progress, in which it is not possible to identify a discrete enhancement.

Although the majority of the enhancements are not substorm onsets, approximately half of them nevertheless occur at some stage within an overall substorm cycle. We therefore determine at what point in the substorm process the enhancement has occurred, by classifying the time of the enhancement into the following categories: growth phase (≤ 30 min before a substorm onset), substorm onset, and expansion/recovery phase (≤ 2 h after substorm onset). Other events that are not deemed to be associated with substorm activity and are classified as “isolated enhancements.”

The universal and magnetic local times of the associated enhancements are determined. The UT value is simply the timestamp of the first image in which the enhancement is clearly visible. The MLT value is the closest MLT, in 15 min intervals, of the approximate center of the enhancement.

An example of a short-lived localized enhancement, which was not associated with any substorm activity, is shown in Figure 1. In each panel is an image of the auroral oval captured by the IMAGE spacecraft, ranging from 03:39 to 03:49 on 15 September 2001. The appearance of the short-lived enhancement ($\tau \approx 8$ min) coincides with an FTFE detection at 03:43. The image taken around the time of the FTFE detection is highlighted by a red outline, and the MLT of the detecting spacecraft (Cluster 2) is shown in that image by a red star. A background level of 1000 counts has been subtracted and the image is saturated at 6000 counts.

The associated solar wind data and in situ plasma and magnetic field data from the Cluster 1 spacecraft are shown in Figure 2. The FTFE detection (indicated by the dashed red line) and associated auroral enhancement seem to coincide approximately with a southward turning in the IMF and precede a small enhancement in the auroral electrojet (AE) index. We note that some uncertainty related to the lagging of the solar wind data from the ACE upstream observer to the bow shock may account for the FTFE being detected slightly before the southward turning appears in the OMNI data [e.g., *Case and Wild*, 2012].

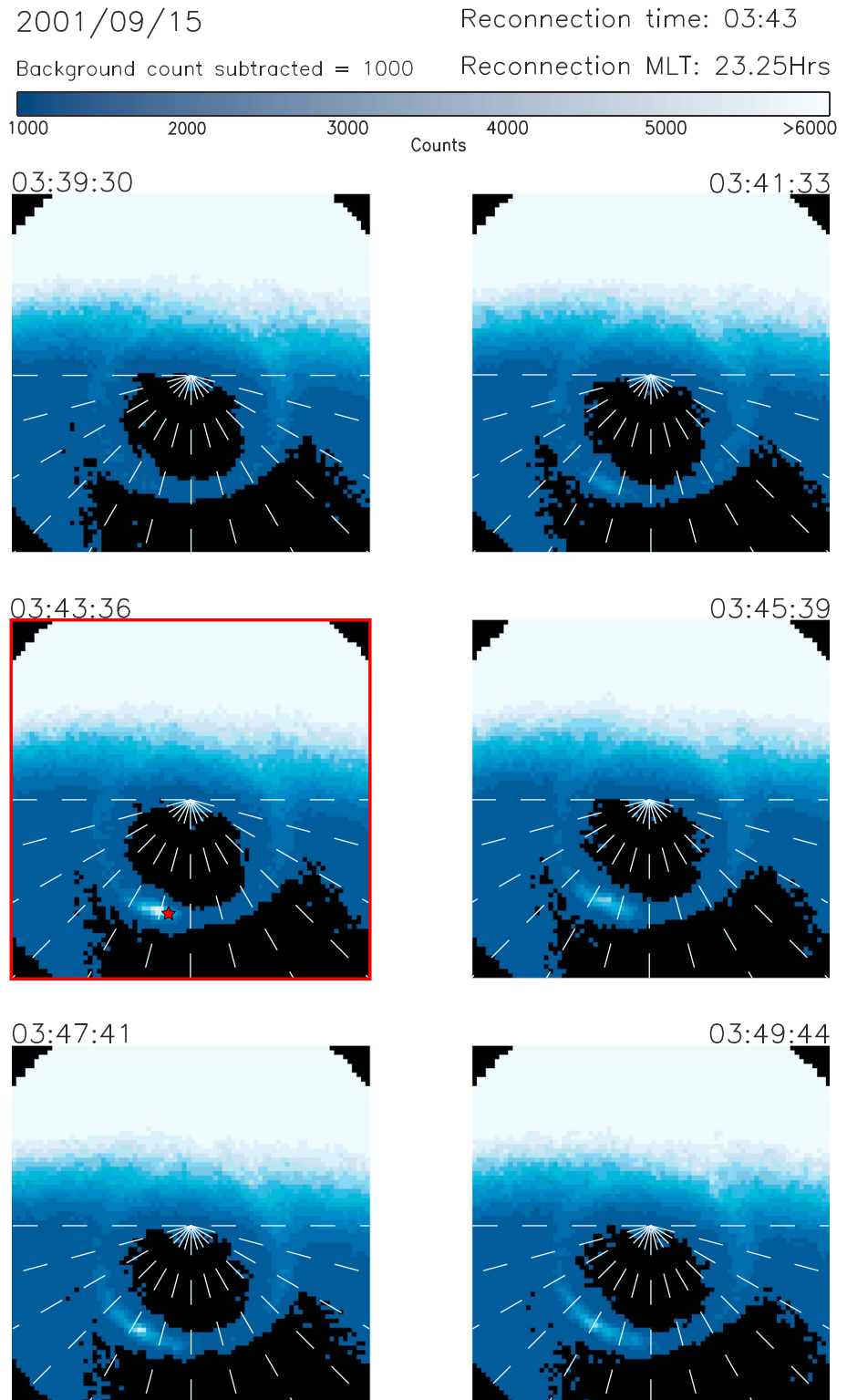


Figure 1. IMAGE FUV WIC data for the period 03:39:30 to 03:49:44 (UT) on 15 September 2001. The appearance of a short-lived localized enhancement in the aurora coincides temporally (UT) and locally (MLT) with the detection of a FTFE in the magnetotail (red star). Dashed lines mark out MLT hours: (left to right) 1800 through 0600.

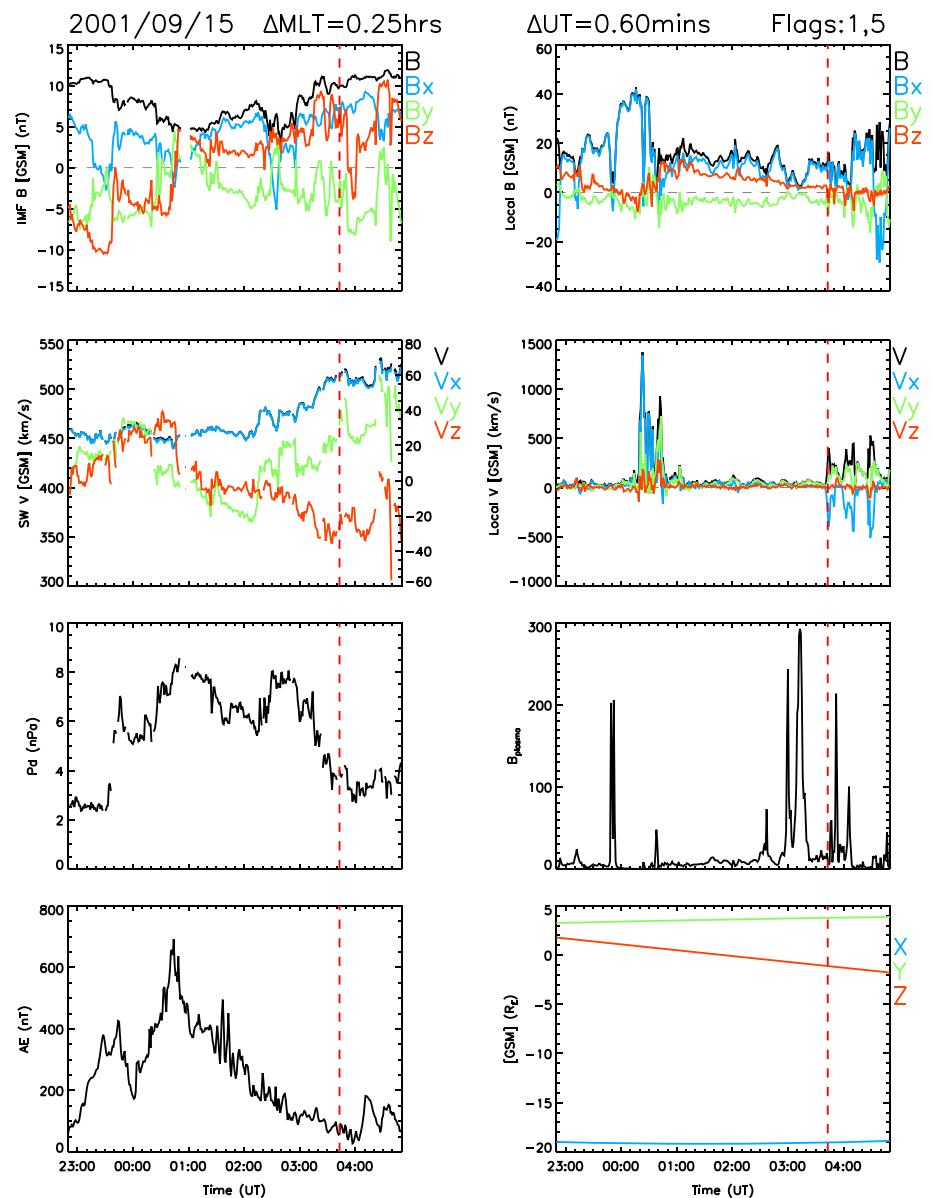


Figure 2. The solar wind and local conditions surrounding the aurora enhancement shown in Figure 1 are shown. In the left column, from top to bottom, (first panel) the IMF components are plotted. (second panel) The solar wind velocity is plotted: (left axis) V magnitude and V_x , (right axis) V_y and V_z . (third panel) The solar wind dynamic pressure and (fourth panel) the auroral electrojet index AE . In the right column, (first panel) the local magnetic field components. (second panel) The local ion velocity. (third panel) The plasma beta and (fourth panel) the spacecraft location. The vertical dashed red lines indicate the time of FTFE detection, and the values at the top of the figure indicate the difference between the timings (in UT and MLT) of the FTFE detection and the aurora enhancement.

The FTFE first detected is followed by two subsequent FTFEs. These two events are excluded from further analysis since they occur within 30 min of the first. We note that the majority of near-Earth FTFEs are singular events and that a group size of three (such as this example) or greater occurs approximately only 25% of the time [Frühhaft and Glasmeier, 2016].

4. Results

As shown in Figure 3, the magnetospheric spacecraft detected 382 FTFEs during the period coinciding with the availability of auroral images (i.e., January 1997 to November 2005). The vast majority of FTFEs were

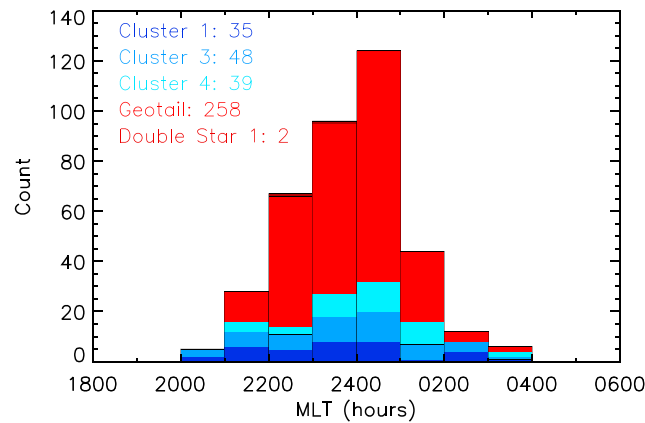


Figure 3. A histogram of the magnetic local time (MLT) of the spacecraft as it first encounters a fast tailward flow magnetic reconnection signature.

detected by the Geotail spacecraft, which is unsurprising owing to its orbital configuration and it being operational throughout this whole time period.

The mean MLT for the FTFE detections is 23.8 h, with the largest bin spanning 2400–0100. This is slightly later than previous studies suggest [e.g., Nagai *et al.*, 1998]; however, Geotail’s orbit post-1999 preferentially samples the dawnside magnetotail [Nagai *et al.*, 2015] and thus later MLT detections are more likely.

Corresponding good quality auroral imaging data were available for 59 of the 382 FTFEs. Of these, a clear and distinct auroral enhancement, such as in Figure 1, could be associated with 43 FTFEs (73%

of events). Thirteen FTFEs (22%) were associated with periods where significant auroral activity was already under way, and it was not possible to associate an individual auroral enhancement with the FTFE. For the remaining three events (5%) no clear auroral enhancement could be associated with the FTFE even with no significant auroral activity currently under way.

Histograms of the time differences between the FTFE detections and the associated auroral enhancements, in both UT and MLT, are shown in Figure 4. Twenty nine of the 43 FTFEs (67%) are detected later in UT than when an enhancement is visible in the aurora. Thirty six (84%) of the FTFE detections are later in MLT than the auroral enhancement location. All but two of the events had a difference of less than ± 90 min in MLT and 81% of events were located within ± 1 h MLT of each other.

In Figure 5, the MLT of the spacecraft as it encounters an FTFE is plotted against the MLT of the auroral enhancement. In Figure 5 (left), each data point is color coded based upon the type of enhancement (see section 3.2 for definitions). The MLTs of the reconnection signatures ($t_{\text{FTFE,MLT}}$) and enhancements ($t_{\text{E,MLT}}$) show a strong positive correlation ($r=0.807$) with the linear line of best fit (shown as the solid black line in the figure) taking the form: $E_{\text{MLT}} = (0.694 \pm 0.079) \times \text{FTFE}_{\text{MLT}} + (6.69 \pm 1.86)$. The “error bars” shown on the plots are estimates of the uncertainty related to both the location of the reconnection event and the auroral enhancement. The x bars represent ± 1 h in MLT, which is simply to acknowledge that the FTFE detection may have been at the outer edge of the reconnection event and not necessarily at the center. The y bars represent ± 15 min in MLT which is related to the uncertainties in determining the exact center of the enhancement.

The most common enhancement type detected (see section 3.2 for definitions) is “short-lived localized enhancement” (60%), followed by “substorm onset” (30%), and “several distinct localized enhancements” (9%).

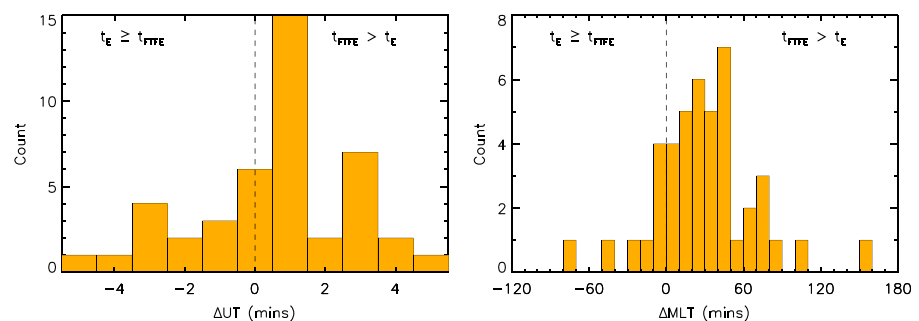


Figure 4. (left) A histogram of the difference in UT between the FTFE (t_{FTFE}) and a corresponding auroral enhancement (t_{E}). (right) A histogram of the difference between the spacecraft MLT as it encounters the FTFE and the enhancement MLT.

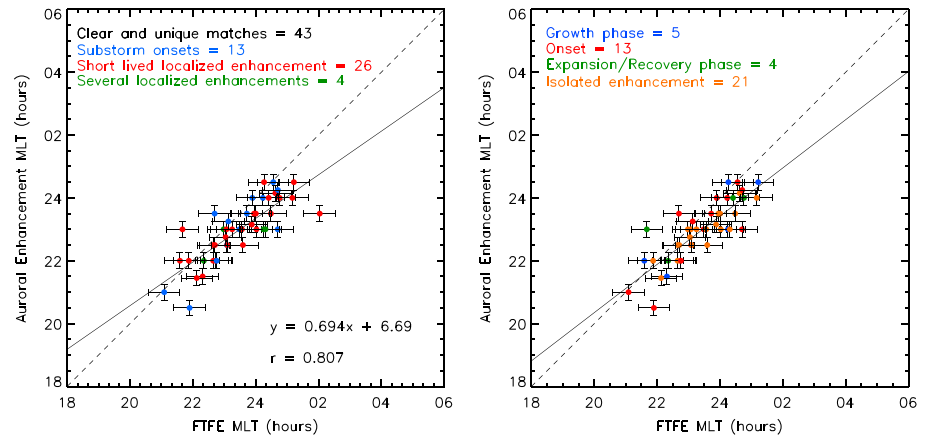


Figure 5. The MLT of the spacecraft as it encounters a reconnection signature is plotted against the MLT of a corresponding aurora enhancement. (left) The data are colored to indicate the type of enhancement. (right) The data are colored to indicate the type of auroral activity associated with the enhancement.

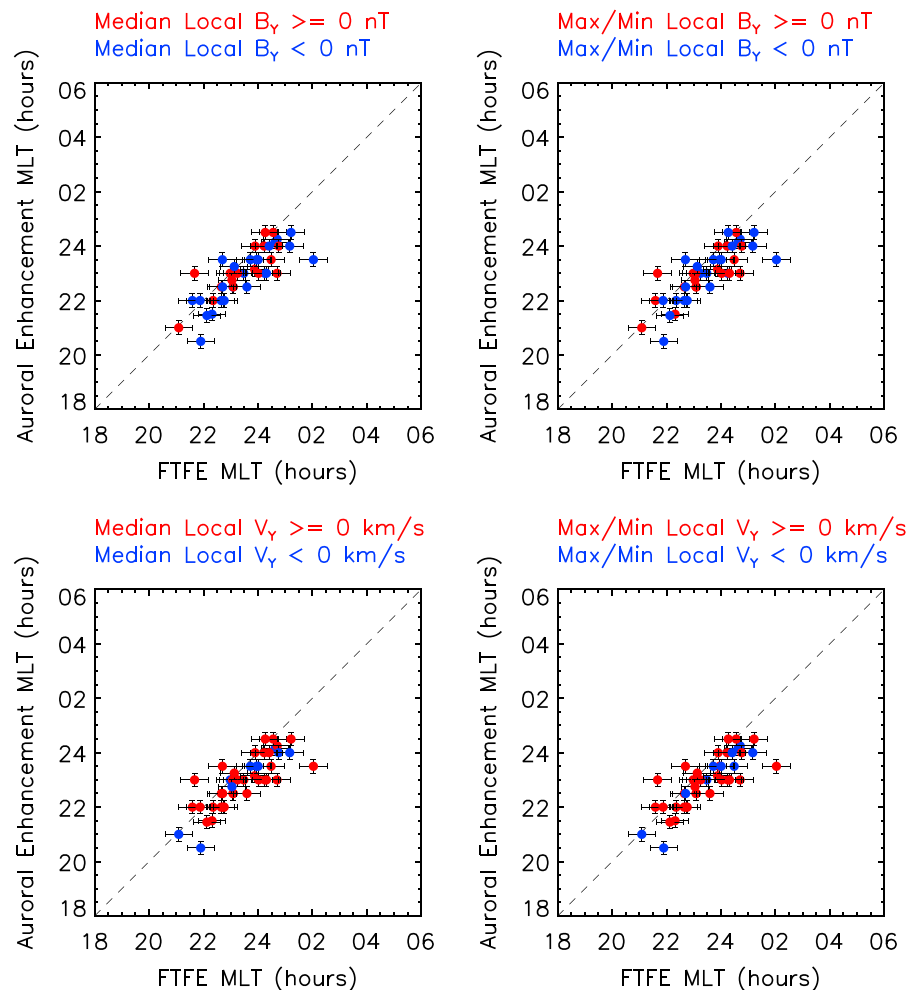


Figure 6. The same data as in Figure 5 are plotted and colored based upon the (top row) y component of the local magnetic field and (bottom row) the y component of the local ion velocity. The panels on the left column are colored using the median values of a 10 min period preceding the FTFE detection of B_y and V_y , respectively, while the panels on the right column are colored using the maximum/minimum values in this period.

Table 1. Mean MLT Location for Auroral Enhancement and Reconnection Under Varying Local and Upstream Conditions

	$B_y < 0$ nT	$B_y \geq 0$ nT	Mean MLT			Δ MLT
			Δ MLT	$V_y < 0$ km/s	$V_y \geq 0$ km/s	
<i>Local Conditions</i>						
Reconnection	23.4	23.4	0.0	23.4	23.4	0.0
Enhancement	22.9	23.0	-0.1	23.4	22.9	0.1
<i>Upstream Conditions</i>						
Reconnection	23.3	23.4	0.1	23.3	23.4	0.1
Enhancement	22.8	23.0	0.2	23.0	22.9	0.1

We find that the short-lived localized enhancements have a lifetime of approximately 10 min or less. They occasionally exhibit some small expansion but never grow beyond 5° in latitude or 30 min in MLT.

Shown in Figure 5 (right) are the data colored by the type of auroral activity associated with the enhancement (see section 3.2 for definitions). The most commonly associated aurora activity type is “isolated enhancement” (49%), followed by substorm “onset” (30%), substorm “growth phase” (12%), and substorm “expansion and recovery phase” (9%).

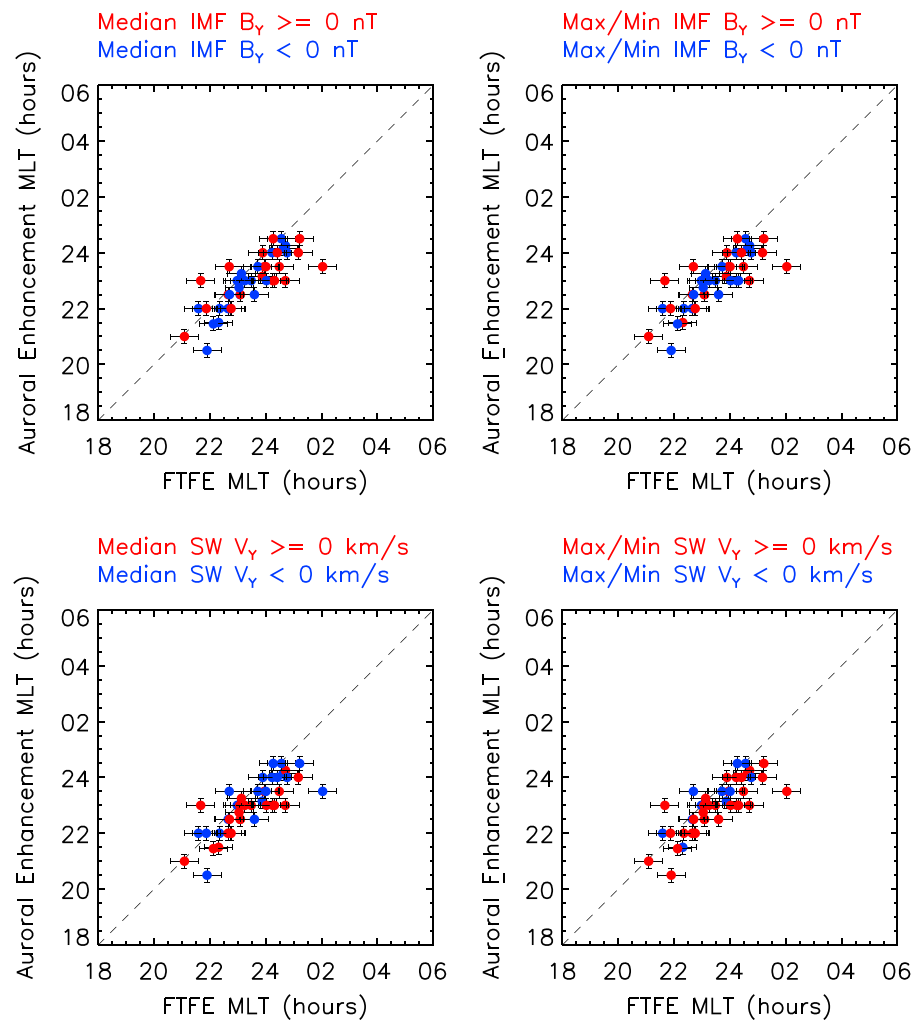


Figure 7. The same data as in Figure 5 are plotted and colored based upon the (top row) y component of the IMF and (bottom row) the y component of the solar wind velocity. The panels on the left column are colored using the median values of B_y and V_y , respectively, while the panels on the right column are colored using the maximum/minimum values.

4.1. Local Conditions

The reconnection and enhancement MLTs are again compared in Figure 6, though the data are now colored using the y component of the associated local (top row) magnetic field and (bottom row) ion velocity. The MLT locations are compared with the y components of these parameters since it is feasible that particularly strong y components may affect the y position (and thus the MLT) of the reconnection site.

In Figure 6 (left column), the median value of the local condition for a 10 min period, immediately preceding the FTFE detection is used; in Figure 6 (right column), the maximum or minimum (whichever has the greater absolute value) in that 10 min period is used. Since the spacecraft can quickly move from region to region, especially the Cluster satellites with their elliptical orbits, a 10 min averaging period prevents “contamination” from other regions while still providing enough data to average (10 points at 1 min cadence).

There appears to be no significant dependence upon the location of the FTFE detection or the auroral enhancement on either the local V_y or B_y components. The mean FTFE/auroral enhancement MLT for $B_y < 0$ nT is found to be 23.3/22.8 h and for $B_y \geq 0$ nT is found to be 23.4/23.0 h. For $V_y < 0$ km/s, the mean location is found to be 23.4/23.1 h and for $V_y \geq 0$ km/s is found to be 23.4/22.9 h. See Table 1 for the summary.

4.2. Upstream Conditions

In Figure 7 (top row), the data are colored by the polarity of the upstream interplanetary magnetic field (IMF) y component (B_y). In the left panel, the median value of a 2 h window of B_y is used to determine the color; in the right panel, the maximum or minimum value (depending on which has the greatest magnitude) in the 2 h window is used. In Figure 7 (bottom row), the data are colored by the orientation of the upstream solar wind velocity y component (V_y). Again, in the left panel, the median value of a 2 h window of V_y is used to determine the color; in the right panel, the maximum or minimum value of the 2 h window is used.

There is no apparent evidence of a significant dependence of the location of the FTFE detection or the auroral enhancement on either the IMF B_y or solar wind V_y shown in Figure 7. The mean FTFE/enhancement for $B_y < 0$ nT is found to be 23.3/22.8 h and for $B_y \geq 0$ nT is found to be 23.4/23.0 h. For $V_y < 0$ km/s, the mean location is found to be 23.3/23.0 h and for $V_y \geq 0$ km/s is found to be 23.4/22.9 h.

The mean MLT values for both the upstream and local conditions are summarized in Table 1.

5. Discussion

In this study, the magnetic reconnection detection criteria of Nagai *et al.* [1998] have been employed to determine reconnection signatures (specifically FTFEs) in the near-Earth magnetotail as recorded by a suite of magnetospheric spacecraft. These detections were then compared to auroral images from two auroral imaging satellite missions with the aim of analyzing the location (in MLT) of the reconnection site and any associated auroral enhancements. This work extends that of previous studies by incorporating data from several spacecraft missions, including two auroral imagers, and using independent criteria for both the enhancement and reconnection identification. Furthermore, the cause of the differences in the location of the auroral enhancements and reconnection sites is explored.

Although the simple fact of two events occurring at a similar time and in a similar place does not necessarily infer causality, it is well known that magnetic reconnection in the magnetotail is associated with various enhancements in the auroral oval. We therefore assume that an auroral enhancement occurring within ± 5 min of the detection of a reconnection signature in the tail is indeed associated with that reconnection event. No criteria on the closeness in MLT was set and yet we find that almost all enhancements (95%) occur within ± 90 min of MLT of the reconnection signature.

In the reconnection region, i.e., ~ 20 – $30 R_E$ downtail of the Earth, 90 min in MLT equates to approximately $10 R_E$. We note, however, that the reconnection region itself is estimated to span approximately $6 R_E$ and thus, a ≤ 90 min MLT difference is not particularly unexpected. We also note that aberration effects, i.e., due to the motion of the Earth, would be relatively minor and might be responsible for a disparity of only ~ 20 min in MLT.

The number of events compared in this study is relatively small, with good quality auroral oval images being available for only 59 of the 382 FTFEs detected. Unfortunately, there is very little that can be done to improve upon this number. Other satellite missions that capture images of the aurora, such as the Defense Meteorological Satellite Program (DMSP) or the Suomi National Polar-orbiting Partnership (Suomi NPP), and

ground-based observers suffer from lack of reliability in capturing the aurora (e.g., due to orbital configuration or cloud cover) or offer only limited spatial coverage of the oval.

Significantly, more good quality auroral images were available for use; however, they did not coincide with an FTFE detection. This is not to say that enhancements in the aurora were not present or that reconnection did not occur during those intervals. Rather, it is simply that the magnetospheric spacecraft employed did not detect the signature of such reconnection. The most likely reason for this is that the spacecraft were not in the right place at the right time. Again, unfortunately, there is nothing that can be done to improve on this.

Of the 59 intervals in which an FTFE was detected and suitable auroral images were available, 56 showed corresponding enhancements in the aurora. However, in 13 of those cases, enhanced auroral activity was already well underway. This meant that it was not possible to determine a unique location for the enhancement that could be associated with the FTFE detection. Further analysis could be undertaken to compare the location of the substorm onset with the FTFE, i.e., by tracing the substorm activity back to its onset, and this may result in the inclusion of these other 13 events.

It might be expected that the FTFE should be detected before the auroral enhancement, since it will take some finite time for the energized magnetospheric particles originally trapped on the now reconnected field to generate the aurora. However, as shown in Figure 4, the UT difference between the FTFE detections and the aurora enhancements was centered around the 0.5–1.5 min bin, with the majority of FTFEs being detected slightly after the enhancement was visible in the aurora. This is consistent with the work of *Ieda et al.* [2001] who suggest that the result is simply due to the distance between the site of reconnection and the spacecraft (which they estimate to be, on average, around $7 R_E$ for their data set). If the spacecraft is indeed several R_E downtail of the reconnection region, several minutes may pass before the FTFE is detected, in which time the auroral brightening may have formed.

We also note that there is some ambiguity in the timings of both the reconnection and auroral enhancements. For example, *Cao et al.* [2006] demonstrated that the start time of fast flows often cannot be accurately determined using one spacecraft alone and there are sometimes a few minutes between start time and detection. Additionally, we note that the auroral enhancement timings are the timestamps of the first image containing that enhancement. The enhancement itself may have appeared milliseconds after the previous image was taken (2 min prior for WIC and 54 s for VIS).

We find that only 30% of the auroral enhancements were a substorm onset, indicating that reconnection occurs without always leading to a substorm, which is consistent with past studies [e.g., *Ieda et al.*, 2001; *Ohtani et al.*, 2002]. The majority of enhancements (60%) are in fact short-lived ($\tau < 10$ min) and do not evolve into any larger activity or expand beyond 5° in latitude or 30 min in MLT. However, just over half of the auroral enhancements do occur at some point during the substorm process (51%). This is somewhat unsurprising, since conditions that are conducive to reconnection in the magnetotail are also conducive to substorm development [e.g., *Angelopoulos et al.*, 2008]. It is also worth noting that unlike PBIs, the localized enhancements we observe do not generally appear at the poleward boundary of the auroral oval and, unlike streamers, do not travel through it. We expect that this is because PBIs tend to be associated with reconnection further downtail which is outside of the region being sampled by the spacecraft used in this study.

Of those auroral enhancements that did occur during the substorm process, 59% were the substorm onset, 23% occurred during the growth phase, and 18% occurred during the expansion/recovery phase. This result indicates that reconnection in the magnetotail plays a role in the buildup to a substorm as well as in the main release of energy from the magnetotail once a substorm has started. Of course, these statistics relate only to reconnection associated with discernible localized auroral enhancements. We expect significant reconnection during the expansion phase associated with the main substorm auroral expansion; however, this would not produce identifiable localized enhancements as there would be too much activity already ongoing.

We note that 49% of auroral enhancements occurred in intervals where there was no other substorm activity present. That is to say that these events appeared to be completely isolated from the substorm process. Individual analysis of these events demonstrated that they were usually accompanied by northward IMF for at least 30 min preceding the enhancement (i.e., conditions that were not favorable for substorm development). As these events demonstrate, reconnection in the near-Earth magnetotail does still occur during northward IMF intervals [*Grocott et al.*, 2003]. Furthermore, we note that substorms can develop during northward IMF turnings, albeit less frequently [*Russell*, 2000].

The locations of both the FTFEs and auroral enhancements range from approximately 21:00 MLT to 02:00 MLT, though the majority were located between 22:00 MLT and 01:00 MLT. This result is consistent with many previous reconnection-related studies, including magnetic field dipolarization at geosynchronous orbit [e.g., Nagai, 1982] and particle injection throughout the equatorial magnetotail [Gabrielse et al., 2014]. The locations were compared with several parameters in Figures 6 and 7 to try to elucidate any reason for the range. No significant trends were found to exist between the local B_y and V_y parameters or the IMF B_y and solar wind V_y parameters. This is in contrast with past studies which did find evidence of solar wind control of the auroral onset location [e.g., Liou et al., 2001; Liou and Newell, 2010; Østgaard et al., 2011]. In those cases the data sets were not limited to coincident auroral and magnetotail observations, and thus had much larger statistics. It is thus likely that if any IMF control does exist, its significance is weak and thus simply not discernible in our relatively small data set.

Finally, we note that three of the FTFEs, in which good auroral imaging data were available, did not show any enhancement in the aurora. This indicates that either the FTFE detection was not actually related to a reconnection event or that the reconnection event did not trigger an observable enhancement in the aurora. The latter has been reported previously [e.g., Milan et al., 2005; Grocott et al., 2007].

6. Conclusions

Comparison of magnetic reconnection signatures, namely, fast tailward flow events (FTFEs), with images of the complete auroral oval (in both nitrogen and oxygen emission-dominated wavelengths) has shown that localized enhancements in the aurora tend to be both temporally and spatially associated with magnetic reconnection in the Earth's magnetotail. The locations, in MLT, of the FTFEs demonstrated a strong positive correlation with the location of the auroral enhancement in the events studied.

The most common type of enhancement found in this study was "short-lived localized enhancement" followed by "substorm onset." Short-lived localized enhancements are enhancements that had a lifetime of less than 10 min, were isolated from other auroral activity (i.e., not part of the substorm process), and had a limited expansion of 5° in latitude and 30 min in MLT. Just over half of the auroral enhancements did occur at some point during the substorm process though, with approximately half of those occurring during the substorm buildup and half occurring during the expansion/recovery phase.

Determining the frequency of magnetic reconnection during each stage of the substorm process, even if complete auroral imaging is not available, seems like a worthwhile extension to this study. Understanding if reconnection events are distributed evenly throughout the substorm process or whether there is some preferred phase, e.g., the expansion phase, in a larger statistical study may elucidate some interesting details about substorm mechanics.

The location of the reconnection signatures and associated aurora enhancements did not seem to show any significant trend with the two parameters tested: B_y and V_y (both locally and solar wind/IMF). Considering that previous studies have shown that the IMF in particular does have an impact on substorms and reconnection, we expect that this null result is simply due to small statistics.

Acknowledgments

We gratefully acknowledge the various instrument teams from each of the spacecraft missions used in this study. The Cluster and Double Star data were provided by ESA's Cluster Science Archive. Data from the other missions were provided by NASA Goddard Space Flight Center's CDAWeb. Solar wind data were provided by NASA GSFC's OMNIWeb database. We thank and acknowledge M. R. Dvorsky, at the University of Iowa, for developing the Polar image analysis code which was adapted and used in this study. N.A.C. and A.G. were supported during this study by STFC grant ST/M001059/1. S.E.M. was supported by STFC grant ST/N000749/1.

References

- Acuña, M. H., K. W. Ogilvie, D. N. Baker, S. A. Curtis, D. H. Fairfield, and W. H. Mish (1995), The Global Geospace Science Program and its investigations, *Space Sci. Rev.*, *71*(1), 5–21, doi:10.1007/BF00751323.
- Akasofu, S. I. (1964), The development of the auroral substorm, *Planet. Space Sci.*, *12*(4), 273–282, doi:10.1016/0032-0633(64)90151-5.
- Angelopoulos, V., W. Baumjohann, C. F. Kennel, F. V. Coroniti, M. G. Kivelson, R. Pellat, R. J. Walker, H. Lühr, and G. Paschmann (1992), Bursty bulk flows in the inner central plasma sheet, *J. Geophys. Res.*, *97*(A4), 4027–4039, doi:10.1029/91JA02701.
- Angelopoulos, V., et al. (2008), Tail reconnection triggering substorm onset, *Science*, *321*(5891), 931–935, doi:10.1126/science.1160495.
- Baker, D. N., T. I. Pulkkinen, V. Angelopoulos, W. Baumjohann, and R. L. McPherron (1996), Neutral line model of substorms: Past results and present view, *J. Geophys. Res.*, *101*(A6), 12,975–13,010.
- Balogh, A., et al. (1997), The cluster magnetic field investigation, in *The Cluster and Phoenix Missions*, edited by C. P. Escoubet, C. T. Russell, and R. Schmidt, pp. 65–91, Springer, Dordrecht, Netherlands, doi:10.1007/978-94-011-5666-0_3.
- Borg, A. L., et al. (2007), Simultaneous observations of magnetotail reconnection and bright X-ray aurora on 2 October 2002, *J. Geophys. Res.*, *112*, A06215, doi:10.1029/2006JA011913.
- Burch, J. L. (2000), Image mission overview, in *The Image Mission*, pp. 1–14, Springer, Dordrecht, Netherlands, doi:10.1007/978-94-011-4233-5_1.
- Cao, J. B., et al. (2006), Joint observations by Cluster satellites of bursty bulk flows in the magnetotail, *J. Geophys. Res.*, *111*, A04206, doi:10.1029/2005JA011322.
- Case, N. A., and J. A. Wild (2012), A statistical comparison of solar wind propagation delays derived from multispacecraft techniques, *J. Geophys. Res.*, *117*, A02101, doi:10.1029/2011JA016946.

- Dungey, J. W. (1961), Interplanetary magnetic field and the auroral zones, *Phys. Rev. Lett.*, *6*(2), 47–48, doi:10.1103/PhysRevLett.6.47.
- Frank, L. A., and J. B. Sigwarth (2003), Simultaneous images of the northern and southern auroras from the Polar spacecraft: An auroral substorm, *J. Geophys. Res.*, *108*(A4), 8015, doi:10.1029/2002JA009356.
- Frank, L. A., J. B. Sigwarth, J. D. Craven, J. P. Cravens, J. S. Dolan, M. R. Dvorsky, P. K. Hardebeck, J. D. Harvey, and D. W. Muller (1995), The Visible Imaging System (VIS) for the polar spacecraft, *Space Sci. Rev.*, *71*(1), 297–328, doi:10.1007/BF00751334.
- Frey, H. U., S. B. Mende, V. Angelopoulos, and E. F. Donovan (2004), Substorm onset observations by IMAGE-FUV, *J. Geophys. Res.*, *109*, A10304, doi:10.1029/2004JA010607.
- Frühauff, D., and K.-H. Glassmeier (2016), Statistical analysis of magnetotail fast flows and related magnetic disturbances, *Ann. Geophys.*, *34*(4), 399–409.
- Gabrielse, C., V. Angelopoulos, A. Runov, and D. L. Turner (2014), Statistical characteristics of particle injections throughout the equatorial magnetotail, *J. Geophys. Res. Space Physics*, *119*, 2512–2535, doi:10.1002/2013JA019638.
- Grocott, A., S. W. H. Cowley, and J. B. Sigwarth (2003), Ionospheric flow during extended intervals of northward but B_y -dominated IMF, *Ann. Geophys.*, *21*, 509–538, doi:10.5194/angeo-21-509-2003.
- Grocott, A., T. K. Yeoman, R. Nakamura, S. W. H. Cowley, H. U. Frey, H. Rème, and B. Klecker (2004), Multi-instrument observations of the ionospheric counterpart of a bursty bulk flow in the near-Earth plasma sheet, *Ann. Geophys.*, *22*, 1061–1075.
- Grocott, A., T. K. Yeoman, S. E. Milan, O. Amm, H. U. Frey, L. Juusola, R. Nakamura, C. J. Owen, H. Rème, and T. Takada (2007), Multi-scale observations of magnetotail flux transport during IMF-northward non-substorm intervals, *Ann. Geophys.*, *25*, 1709–1720, doi:10.5194/angeo-25-1709-2007.
- Hones, E. W., Jr. (1979), Plasma flow in the magnetotail and its implications for substorm theories, in *Dynamics of the Magnetosphere*, edited by S. I. Akasofu, pp. 545–562, Springer, Netherlands.
- Ieda, A., S. Machida, T. Mukai, Y. Saito, T. Yamamoto, A. Nishida, T. Terasawa, and S. Kokubun (1998), Statistical analysis of the plasmoid evolution with Geotail observations, *J. Geophys. Res.*, *103*(A3), 4453–4465, doi:10.1029/97JA03240.
- Ieda, A., D. H. Fairfield, T. Mukai, Y. Saito, S. Kokubun, K. Liou, C.-I. Meng, G. K. Parks, and M. J. Brittnacher (2001), Plasmoid ejection and auroral brightenings, *J. Geophys. Res.*, *106*(A3), 3845–3857, doi:10.1029/1999JA000451.
- Ieda, A., et al. (2008), Longitudinal association between magnetotail reconnection and auroral breakup based on Geotail and Polar observations, *J. Geophys. Res.*, *113*, A08207, doi:10.1029/2008JA013127.
- Kokubun, S., T. Yamamoto, M. H. Acuña, K. Hayashi, K. Shiokawa, and H. Kawano (1994), The Geotail magnetic field experiment, *J. Geomagn. Geoelectr.*, *46*(1), 7–22.
- Liou, K. (2010), Polar Ultraviolet Imager observation of auroral breakup, *J. Geophys. Res.*, *115*, A12219, doi:10.1029/2010JA015578.
- Liou, K., and P. T. Newell (2010), On the azimuthal location of auroral breakup: Hemispheric asymmetry, *Geophys. Res. Lett.*, *37*, L23103, doi:10.1029/2010GL045537.
- Liou, K., P. T. Newell, D. G. Sibeck, C.-I. Meng, M. Brittnacher, and G. Parks (2001), Observation of IMF and seasonal effects in the location of auroral substorm onset, *J. Geophys. Res.*, *106*(A4), 5799–5810, doi:10.1029/2000JA003001.
- Liu, Z. X., C. P. Escoubet, Z. Pu, H. Laakso, J. K. Shi, C. Shen, and M. Hapgood (2005), The Double Star mission, *Ann. Geophys.*, *23*(8), 2707–2712, doi:10.5194/angeo-23-2707-2005.
- Lyons, L. R., T. Nagai, G. T. Blanchard, J. C. Samson, T. Yamamoto, T. Mukai, A. Nishida, and S. Kokubun (1999), Association between Geotail plasma flows and auroral poleward boundary intensifications observed by CANOPUS photometers, *J. Geophys. Res.*, *104*(A3), 4485–4500, doi:10.1029/1998JA900140.
- McPherron, R. L. (2016), Where and when does reconnection occur in the tail?, *J. Geophys. Res.*, *121*, 4607–4610, doi:10.1002/2015JA022258.
- Mende, S. B., et al. (2000), Far ultraviolet imaging from the image spacecraft. 2. Wideband FUV imaging, in *The Image Mission*, edited by J. L. Burch, pp. 271–285, Springer, Dordrecht, Netherlands, doi:10.1007/978-94-011-4233-5_9.
- Milan, S. E., B. Hubert, and A. Grocott (2005), Formation and motion of a transpolar arc in response to dayside and nightside reconnection, *J. Geophys. Res.*, *110*, A01212, doi:10.1029/2004JA010835.
- Milan, S. E., A. Grocott, and B. Hubert (2010), A superposed epoch analysis of auroral evolution during substorms: Local time of onset region, *J. Geophys. Res.*, *115*, A00104, doi:10.1029/2010JA015663.
- Mukai, T., S. Machida, Y. Saito, M. Hirahara, T. Terasawa, N. Kaya, T. Obara, M. Ejiri, and A. Nishida (1994), The Low Energy Particle (LEP) experiment onboard the Geotail satellite, *J. Geomagn. Geoelectr.*, *46*(1), 669–692.
- Nagai, T. (1982), Observed magnetic substorm signatures at synchronous altitude, *J. Geophys. Res.*, *87*(A6), 4405–4417, doi:10.1029/JA087iA06p04405.
- Nagai, T., M. Fujimoto, Y. Saito, S. Machida, T. Terasawa, R. Nakamura, T. Yamamoto, T. Mukai, A. Nishida, and S. Kokubun (1998), Structure and dynamics of magnetic reconnection for substorm onsets with Geotail observations, *J. Geophys. Res.*, *103*(A3), 4419–4440, doi:10.1029/97JA02190.
- Nagai, T., M. Fujimoto, R. Nakamura, W. Baumjohann, A. Ieda, I. Shinohara, S. Machida, Y. Saito, and T. Mukai (2005), Solar wind control of the radial distance of the magnetic reconnection site in the magnetotail, *J. Geophys. Res.*, *110*, A09208, doi:10.1029/2005JA011207.
- Nagai, T., I. Shinohara, M. Fujimoto, A. Matsuoka, Y. Saito, and T. Mukai (2011), Construction of magnetic reconnection in the near-Earth magnetotail with Geotail, *J. Geophys. Res.*, *116*, A04222, doi:10.1029/2010JA016283.
- Nagai, T., I. Shinohara, and S. Zenitani (2015), The dawn-dusk length of the X line in the near-Earth magnetotail: Geotail survey in 1994–2014, *J. Geophys. Res. Space Physics*, *120*, 8762–8773, doi:10.1002/2015JA021606.
- Nakamura, R., W. Baumjohann, R. Schödel, M. Brittnacher, V. A. Sergeev, M. Kubyshkina, T. Mukai, and K. Liou (2001), Earthward flow bursts, auroral streamers, and small expansions, *J. Geophys. Res.*, *106*(A6), 10,791–10,802, doi:10.1029/2000JA000306.
- Nishida, A., and N. Nagayama (1973), Synoptic survey for the neutral line in the magnetotail during the substorm expansion phase, *J. Geophys. Res.*, *78*(19), 3782–3798, doi:10.1029/JA078i019p03782.
- Nishida, A., H. Hayakawa, and E. W. Hones Jr. (1981), Observed signatures of reconnection in the magnetotail, *J. Geophys. Res.*, *86*(A3), 1422–1436, doi:10.1029/JA086iA03p01422.
- Ohtani, S., R. Yamaguchi, M. Nosé, H. Kawano, M. Engebretson, and K. Yumoto (2002), Quiet time magnetotail dynamics and their implications for the substorm trigger, *J. Geophys. Res.*, *107*(A2), 1030, doi:10.1029/2001JA000116.
- Østgaard, N., K. M. Laundal, L. Juusola, A. Åsnes, S. E. Håland, and J. M. Weygand (2011), Interhemispherical asymmetry of substorm onset locations and the interplanetary magnetic field, *Geophys. Res. Lett.*, *38*, L08104, doi:10.1029/2011GL046767.
- Reistad, J. P., N. Østgaard, P. Tenfjord, K. M. Laundal, K. Snekvik, S. Haaland, S. E. Milan, K. Oksavik, H. U. Frey, and A. Grocott (2016), Dynamic effects of restoring footpoint symmetry on closed magnetic field lines, *J. Geophys. Res. Space Physics*, *121*, 3963–3977, doi:10.1002/2015JA022058.
- Rème, H., et al. (2001), First multispacecraft ion measurements in and near the Earth's magnetosphere with the identical Cluster Ion Spectrometry (CIS) experiment, *Ann. Geophys.*, *19*, 1303–1354, doi:10.5194/angeo-19-1303-2001.

- Russell, C. T. (2000), How northward turnings of the IMF can lead to substorm expansion onsets, *Geophys. Res. Lett.*, *27*(20), 3257–3259.
- Tsyganenko, N. A., and M. I. Sitnov (2005), Modeling the dynamics of the inner magnetosphere during strong geomagnetic storms, *J. Geophys. Res.*, *110*, A03208, doi:10.1029/2004JA010798.
- Zenitani, S., I. Shinohara, and T. Nagai (2012), Evidence for the dissipation region in magnetotail reconnection, *Geophys. Res. Lett.*, *39*, L11102, doi:10.1029/2012GL051938.
- Zhang, Q.-H., et al. (2010), Simultaneous observations of reconnection pulses at Cluster and their effects on the cusp aurora observed at the Chinese Yellow River Station, *J. Geophys. Res.*, *115*, A10237, doi:10.1029/2010JA015526.